**Proceedings of GT2006**
**ASME Turbo Expo 2006: Power for Land, Sea, and Air**
**May 8-11, 2006, Barcelona, Spain**

# GT2006-90194

## COMPARISON OF RECUPERATOR ALLOY DEGRADATION IN LABORATORY AND ENGINE TESTING

**Bruce A. Pint, Karren L. More, Rosa Trejo and Edgar Lara-Curzio**
Oak Ridge National Laboratory
Metals and Ceramics Division
Oak Ridge, Tennessee 37831-6156
Phone: (865) 576-2897, E-mail: pintba@ornl.gov

### ABSTRACT

In order to increase the efficiency of advanced microturbines, durable alloy foils are needed for their recuperators to operate at 650°-700°C. Prior work has demonstrated that water vapor in the exhaust gas causes more rapid consumption of Cr from austenitic alloys leading to a reduction in lifetime for the thin-walled components in this application. New commercial alloy foils are being tested in both laboratory tests in humid air and in the exhaust gas of a modified 60kW microturbine. Initial results are presented for a commercial batch of 80μm alloy 120 foil. The Cr consumption rates in laboratory testing were similar to those observed in previous testing. The initial results from the microturbine indicate a faster Cr consumption rate compared to the laboratory test but longer term results are needed to quantify the difference. These results will help to verify a Cr consumption model for predicting lifetimes in this environment based on classical gas transport theory.

### INTRODUCTION

Distributed generation is an attractive solution both for energy security and energy efficiency demands. In cases of transmission line failure, natural disaster or terrorist events, the capability for on-site power generation can maintain a variety of critical services including communications and medical care. While reciprocating engines have long met this need, small (25-300kW) gas turbines or microturbines[1,2] offer an additional potential advantages due to their fuel flexibility, lower emissions and use of waste heat (i.e. combined heat and power[3,4]) which greatly increases their overall efficiency.

Two problems limiting marketplace acceptance of microturbines are cost and electrical efficiency (currently <30%), especially in the current environment of increasing fuel costs. Due to the relatively small size and single shaft design of most microturbines, there are not many opportunities for improving their efficiency except by increasing the recuperator (i.e. heat exchanger) efficiency or by increasing the turbine inlet temperature, which also increases the recuperator operating temperature.[5]

There are a number of different recuperator designs but most employ thin-walled components in order to maximize specific heat transfer.[5-7] The most widely used material has been type 347 stainless steel foil (~100μm thick, composition in Table I) because of its excellent combination of creep and corrosion resistance. However, over the past decade it has become clear that, for recuperator temperatures above ~590°C (1100°F), serious durability problems have been encountered for type 347 foils.[8-10] It is now widely recognized that this accelerated degradation in exhaust gas is due to the presence of water vapor and that all chromia-forming alloys exhibit greater degradation in the presence of water vapor due to the volatilization of the oxy-hydroxide, $CrO_2(OH)_2$.[11,12]

In the past few years, a number of replacement materials have been investigated and implemented. For example, alloy 625 is being used in the recuperator of a 4MW engine[13] and alloy 120 is being studied for use in a 200kW microturbine.[14] A less expensive alternative material is Nb-modified Fe-20Cr-25Ni, which had been developed in the 1950's by the British nuclear materials program and subsequently was developed as a tube alloy, 709.[15] This material is now commercially available in foil form.[16] However, it was recently demonstrated that all of these advanced alloys lose Cr at approximately the same rate during laboratory exposures in humid air at 650°-700°C, seemingly independent of Cr, Ni or Mn content.[17] Furthermore, even with their high Cr and Ni contents, the Fe-base alloys in foil form, 120 and 709, formed Fe-rich oxide nodules at 650°C. The reason for

Table I. Alloy chemical compositions (weight %) and average grain sizes (μm) of the foil and sheet materials.

| | Cr | Ni | Mn | Si | Other | Grain Size (μm) |
|---|---|---|---|---|---|---|
| Type 347 | 17.8 | 9.9 | 1.6 | 0.5 | 0.5Nb | 5 |
| 709 | 20.3 | 24.7 | 1.0 | 0.4 | 1.5Mo,0.2Nb | 16 |
| 20/25+Nb | 20.3 | 25.4 | 1.1 | 0.3 | 1.5Mo,0.4Nb | 11 |
| 120 | 24.7 | 37.6 | 0.7 | 0.2 | 0.3Mo,0.6Nb | 23 |
| 625 | 23.1 | 63.8 | 0.04 | 0.2 | 8.9Mo, 4Nb, 3Fe | 12 |

the nodule formation was that the near-surface region, and particularly the alloy grain boundaries, became depleted in Cr because of evaporation of the reaction product and the diffusion of Cr in the alloy at that temperature is not fast enough to resupply the surface. Extrapolation of the Cr loss rates measured after 10,000h exposures to the desired 40,000h minimum service life indicated potential problems for all of these alloys. However, there is no correlation data available between laboratory and actual recuperator exposures. This paper reports the initial comparison results of Cr depletion from commercial 80μm foil alloy 120 exposed in laboratory testing and in the exhaust gas of a modified 60kw microturbine.[18] Due to the short duration of the microturbine exposure (1,000h), it is difficult to quantify the difference between the two tests. Qualitatively, it appears that the depletion is much more significant in the exhaust gas compared to the laboratory test.

## EXPERIMENTAL PROCEDURE

The material tested in this study was commercially fabricated 80μm alloy 120 foil with an average grain size of 23μm, Figure 1. Chemical composition from a piece of bulk alloy 120 material is provided in Table I. For comparison, results from other commercial foils also are included.

For the laboratory test, specimens (~1 x 12 x 18mm) were tested in the as-rolled condition and were cleaned in acetone and methanol prior to oxidation. Mass changes were measured using a Mettler-Toledo model AG245 balance. Exposures were 100h cycles at 650°, 700° or 800°C. Oxidation exposures in humid air were conducted by flowing the gas at 850cc/min through an alumina tube that was inside a resistively-heated tube furnace. Distilled water was atomized into the flowing gas stream above its condensation temperature and heated to the reaction temperature within the alumina tube. The amount of water flowing through the tube was measured to calculate its concentration and calibrate the amount of injected water. A water content of 10±1 vol.% was used for these experiments. Up to 40 specimens were positioned in alumina boats in the furnace hot zone so as to expose the specimen faces to the flowing gas. For testing in air, the alumina furnace tubes were not sealed.

The engine exposures were conducted in a modified 60kW Capstone Turbine Corp. microturbine located at ORNL. The turbine was modified to allow higher turbine exit temperatures and placement of six ports at the entrance to the recuperator where specimen holders can be inserted. Details of the port locations and specimen holder are provided elsewhere.[18,19] Foil specimens were formed with a 23.1mm diameter and were laser welded onto four locations on the holder with one thermocouple at each location. The temperature along the holder varied from 720° to 600°C. The foils were internally pressurized at 0.4MPa (60psi) resulting in a ~50MPa stress in the foil. This reproduces the stress state in a primary surface recuperator during typical operation where the foil has compressed inlet air on one side and exhaust gas at near ambient pressure on the other side.

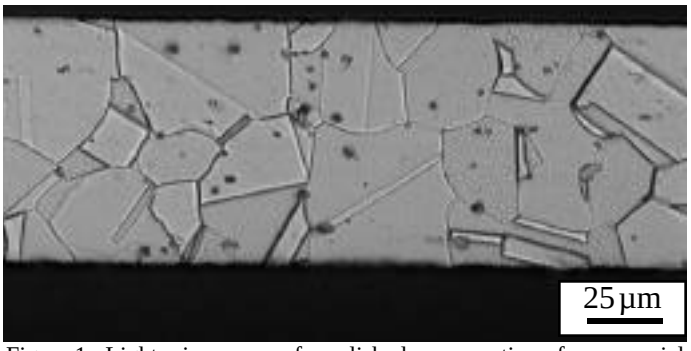


Figure 1. Light microscopy of a polished cross-section of commercial as-received 80μm alloy 120 foil.

After oxidation, specimens were Cu-plated or mounted directly in epoxy and sectioned for metallographic analysis and electron probe microanalysis (EPMA) to determine Cr depletion. In general, three composition profiles across the foil thickness were performed with a 1μm step size and summed to determine the residual Cr content in the specimen.

## RESULTS

### Laboratory Testing in Humid Air

Specimens of two commercial foils, alloys 120 and 20/25+Nb, are being tested under the same conditions as prior work[10,17] at 650°, 700° and 800°C. An example of the mass gain data is shown in Figure 2. For comparison, the mass gain for commercial type 347 foil is shown where an accelerated mass gain was observed after less than 2,000h of testing at 650°C. The new batches of commercially rolled material are showing similar mass gain behavior as the previous laboratory rolled foils with similar compositions, Table I. However, the information that can be learned from the specimen mass gain data is limited because it is the summation of several mechanisms, including oxide scale growth, evaporation and spallation of the scale:

$$\Delta M_{specimen} = \Delta M_{oxide\ growth} - \Delta M_{evap.} - \Delta M_{spall}$$

In this work there was no evidence of scale spallation so oxide growth and oxy-hydroxide evaporation are summed in the data. In general, the mass gain can be used to identify the onset of accelerated attack but is not very useful in quantifying the amount of Cr lost because of these competing factors.

Individual specimens of 80μm alloy 120 foil were stopped after

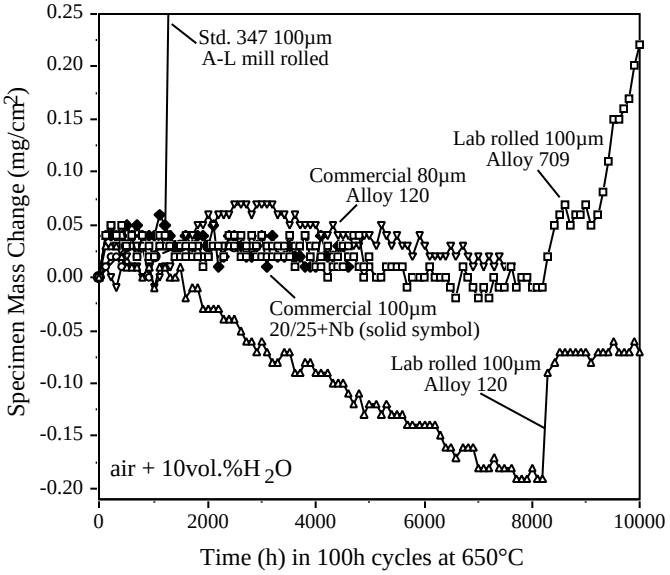


Figure 2. Specimen mass gains for various foil materials during 100h cycles in humid air at 650°C.

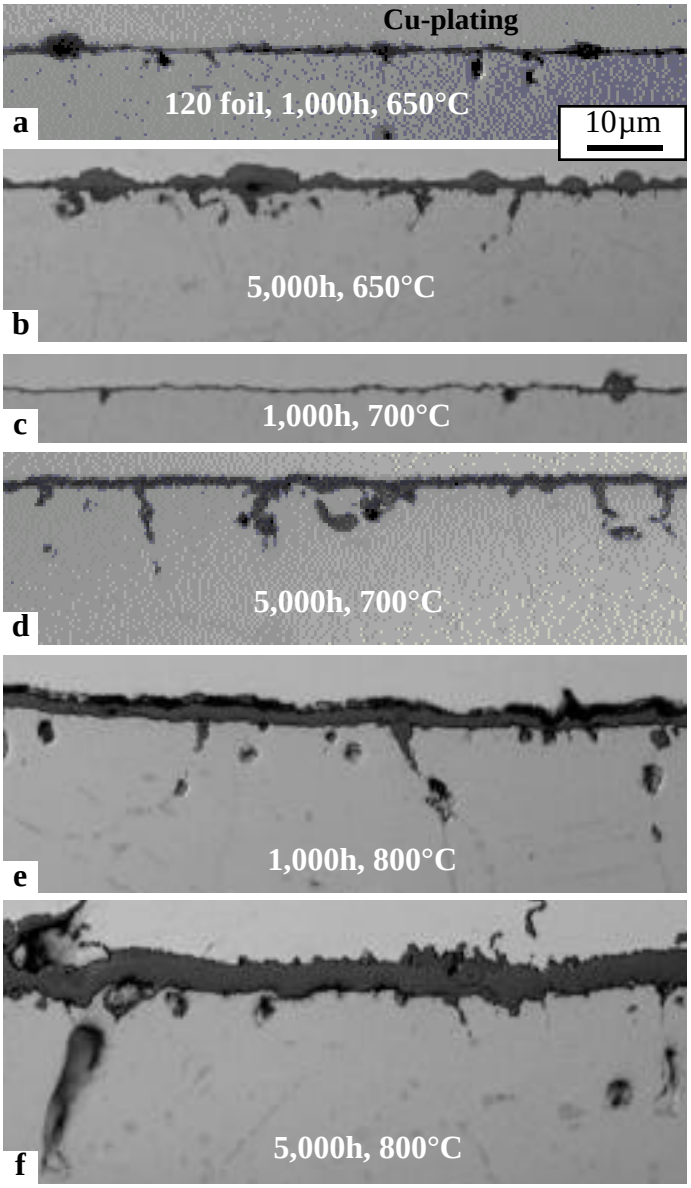


Figure 3. Light microscopy of polished cross-sections of 80µm alloy 120 foil oxidized in humid air for (a) 1,000h at 650°C, (b) 5,000h at 650°C, (c) 1,000h at 700°C, (d) 5,000h at 700°C, (e) 1,000h at 800°C, and (f) 5,000h at 800°C.

1,000 and 5,000h for characterization. Figure 3 shows polished cross-sections of these specimens. In general, the oxide increased in thickness with time and temperature. However, the oxide appeared slightly thinner at 700°C compared to 650°C, Figures 3a and 3c. At all conditions, internal penetrations were observed. At 650°C, a few small Fe-rich oxide nodules had begun to form, Figures 3a and 3b.

To illustrate the effect of water vapor on the oxidation of this material, Figure 4 shows a comparison after 10,000h exposures at 700°C for 90µm commercial alloy 120 foil. The specimen exposed in laboratory air (Figure 4b) had a much thinner oxide scale than the specimen exposed in humid air (Figure 4a). However, occasional penetrations and small nodules were observed.

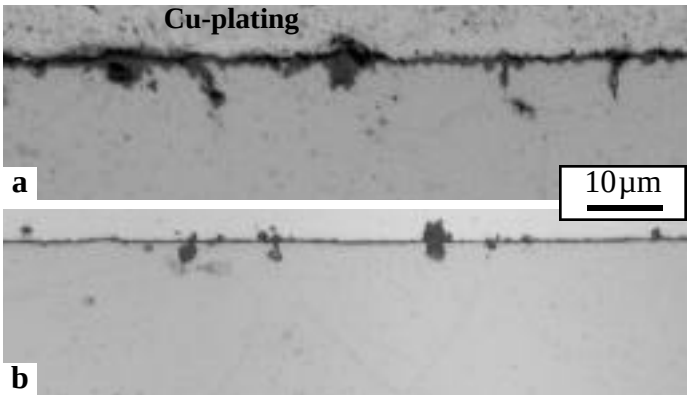


Figure 4. Light microscopy of polished cross-sections of 90µm alloy 120 foil oxidized for 10,000h at 700°C in (a) humid air and (b) laboratory air.

**Microturbine Exposures**

A set of alloy 120 foil specimens were removed from the microturbine specimen holder after 1,000h. Figure 5 shows polished cross-sections for the specimens exposed at the four specimen holder locations with temperatures of 720°, 690°, 670° and 600°C. As with

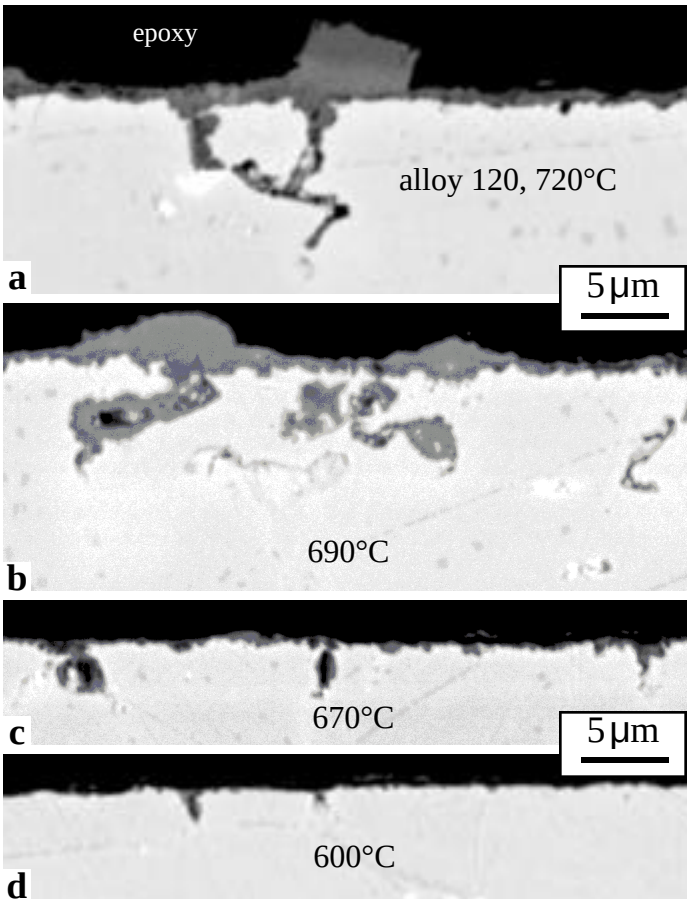


Figure 5. Secondary electron images of polished cross-sections of alloy 120 foil exposed for 1,000 in the exhaust gas of a 60kW microturbine. The specimens were exposed at (a) 720°C, (b) 690°C, (c) 670°C and (d) 600°C.

the laboratory exposures, internal penetrations were observed at each temperature. Nodule formation was observed at the higher temperatures. A very thin reaction product was observed at the two lower temperatures. While these temperatures were not exactly the same as those in the laboratory test, comparing Figures 3a, 3c and 5, the scale thicknesses in the two tests after 1,000h do not correlate particularly well with temperature.

## Characterization by EPMA

To quantify the relative Cr depletion in the two tests, composition profiles were measured using EPMA. Figure 6 gives example profiles for some of the foils shown in Figure 3. (The EPMA profiles are in at.% so the Cr contents are higher than the wt.% in Table I.) Chromium depletion was concentrated near the specimen surface with the Cr composition at the center of the foil remaining relatively unchanged. Occasional peaks in the profiles are attributed to Cr-rich carbides.[20] As with the oxide thickness, the amount of Cr depletion did not increase with temperature between 650° and 700°C. The depletion after exposure for 5,000h at 650°C (Figure 6a) was much more distinct than that observed after 5,000h at 700°C. At 800°C, a large amount of depletion was observed after only 1,000h, Figure 6d. The depletion in each case was fairly uniform on both sides of the specimen.

For the specimens exposed to the microturbine, the profiles were less pronounced due to the relatively short exposure. Figure 7 shows profiles from the highest temperature, 720°C, after 1,000h. Only one side of the specimen was exposed to the exhaust gas and, as expected, this side showed more Cr depletion. One of the profiles showed more depletion than the other (arrow in Figure 7), due to intersection with one of the alloy grain boundaries. As shown previously, at 650°-700°C, the Cr depletion is higher on alloy grain boundaries near the surface due to increased Cr diffusion along these boundaries. To illustrate this, Figure 8 shows EPMA Cr and O maps from three of the microturbine exposures. The Cr maps show the surface oxide scale on both sides is enriched in Cr as are the alloy grain boundaries due to carbide formation. However, near the surface exposed to exhaust gas (top of each map), the alloy grain boundaries go from enriched (bright) to depleted (dark). In several cases, oxide has penetrated down the grain boundaries and Fe-rich oxide nodules (arrows in O maps) tend to nucleate above depleted alloy grain boundaries. On the side not exposed to the exhaust gas, no nodules or penetrations were observed. These depletion observations are very similar to those reported previously for foils of alloys 709, 120 and 625.[17] Thus, the less-depleted profile in Figure 7 was not near an alloy grain boundary while the other was on a boundary.

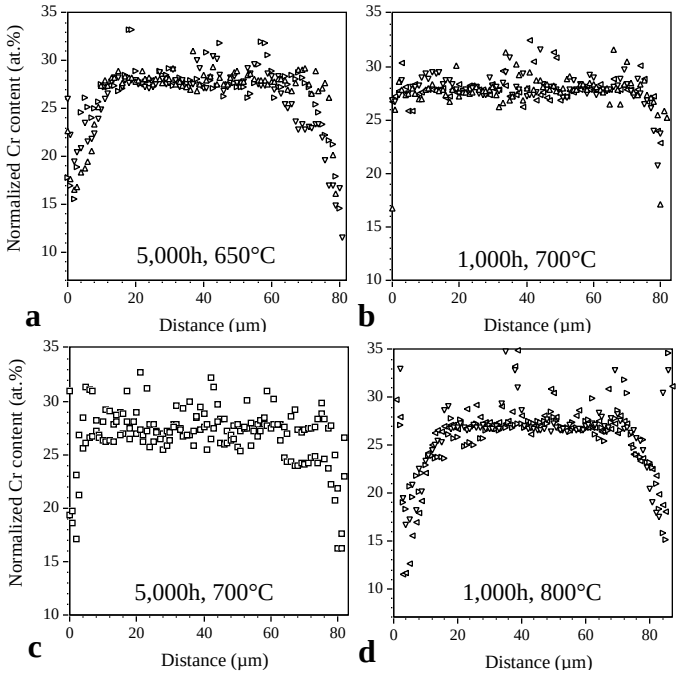


Figure 6. EPMA Cr profiles from three scans across the cross-section of alloy 120 foils after laboratory exposures in humid air for (a) 5,000h at 650°C, (b) 1,000h at 700°C (c) 5,000h at 700°C and (d) 1,000h at 800°C.

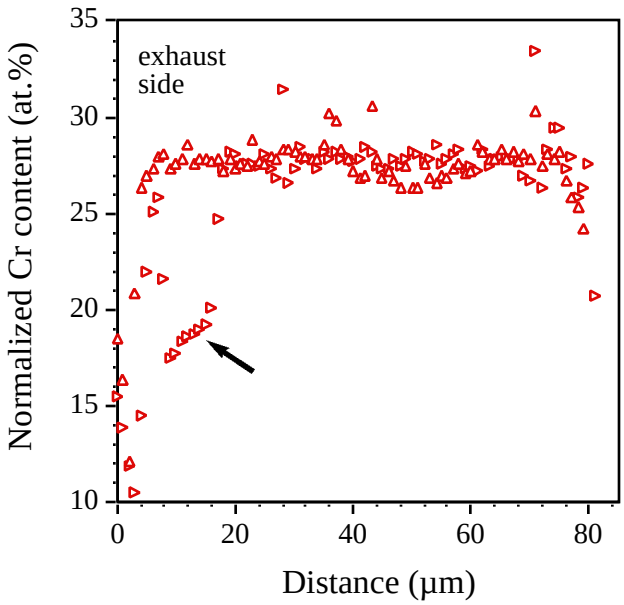


Figure 7. EPMACr profiles from two scans across the cross-section of alloy 120 foil after exposures in a microturbine recuperator for 1,000h at 720°C. The side exposed to the exhaust gas is marked.

To quantify the Cr depletion, the profiles were used to determine the remaining metal thickness and the Cr content at each 1μm increment was summed and compared to profiles from the starting thickness and Cr content to determine the amount of Cr lost. Table II summarizes some previously obtained results after 10,000h laboratory exposures in humid air where the depletion layer was very distinct. After 10,000h, the Cr depletion in alloy 120 specimens increased with temperature from 650°-800°C.

In the shorter term exposures in this study, the summation did not yield a statistically significant depletion after many of the 1,000h exposures. Even the 5,000h exposure at 700°C only showed a small depletion. Figure 9 summarizes the depletions that were measurable and their standard deviations. These points are plotted along with the previous 10,000h data points for alloy 120 foils and the lines fit the data at each condition. For the laboratory exposures, substantial depletion was observed after 5,000h at 650°C, where more distinct depletion profiles were evident, Figure 6a, and for 1,000h and 5,000h exposures at 800°C. For comparison to the data in humid air, an alloy 120 foil specimen exposed for 5,000h in laboratory air showed 1/3 less Cr depletion without water vapor.

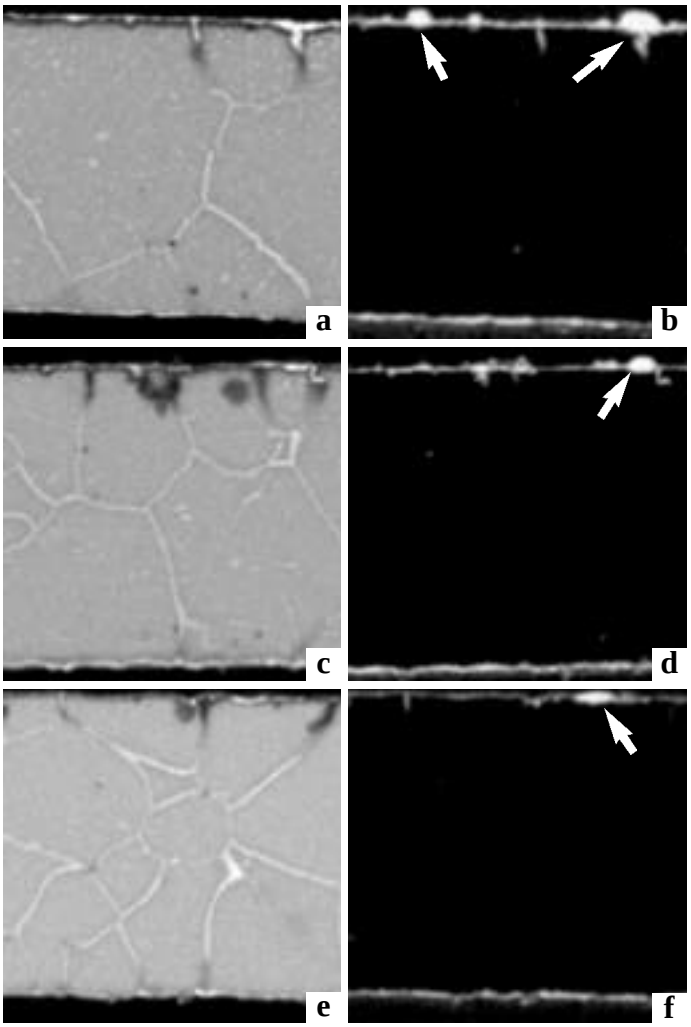


Figure 8. EPMACr (a,c,e) and O (b,d,f) maps of 80µm alloy 120 foil after 1,000h exposures in exhaust gas at (a,b) 720°C, (c,d) 690°C, and (e,f) 670°C. The exhaust gas side is up in these images.

The foil exposed to exhaust gas for 1,000h at 720°C was the only specimen from the microturbine to show a significant depletion. The exposures at lower temperatures did not show distinct profiles like this specimen, Figure 7. However, because the two profiles were so different, a very high standard deviation was obtained. Additional profiles need to be measured to obtain a more accurate assessment of the Cr depletion in this specimen.

Table II. Amount of Cr consumed (wt.%) for various foil materials oxidized in humid air for 10,000 h (except where noted). The standard deviation for three EPMA profiles is shown.

| Alloy | 650°C | 700°C | 800°C |
|---|---|---|---|
| 709 | -1.7±1.0% | -2.2±0.8% | -10.2±0.5%* |
| 120 (ORNL roll) | -2.0±0.3% | -2.7±0.6% | |
| 120 (Commercial) | | -2.5±0.9% | -12.2±0.3% |

* after 6,000h

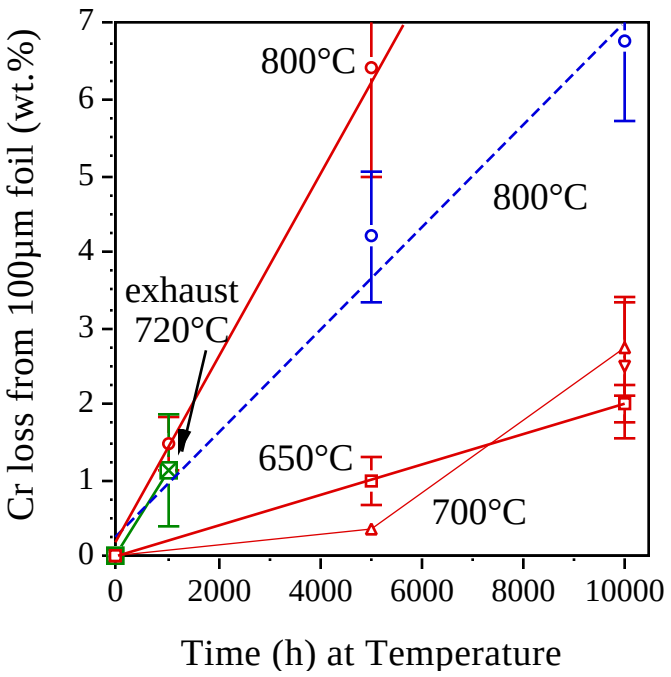


Figure 9. Chromium mass losses from alloy 120 foil specimens as a function of time after exposures to air + 10%$H_2O$ (solid lines) at 650°-800°C and exhaust gas at 720°C. Values for 800°C exposures in laboratory air (dashed line)are shown for comparison.

## Model Development

The first step in the development of a lifetime model was completed by applying classical gas transport theory to the Cr evaporation assuming the evaporation of $CrO_2(OH)_2$ occurs by the reaction:

$$1/2\ Cr_2O_3(s) + 3/4\ O_2(g) + H_2O(g) = CrO_2(OH)_2(g) \quad [1]$$

Details of this analysis are available elsewhere.[21] The experimental Cr depletion results for alloy 709 foil specimens[17] were compared to calculations based on recent $CrO_2(OH)_2$ thermodynamic data from E. Opila at NASA Glenn Research Center. By using the experimental gas composition, specimen length (*l*) and velocity (v), a good match was obtained between the calculation and the experimental results, Figure 10. Thus it is reasonable to assume that this evaporation mechanism is responsible for the Cr loss and the accelerated corrosion observed in the recuperator.

The next step in the model development was to perform the same calculations based on the recuperator conditions. One of the most important variables for this calculation was the v/*l* ratio and its effect on the Cr loss flux, $J_{Cr}$, at several temperatures, as shown in Figure 11. The expected v/*l* ratio in the recuperator is marked as well as the conditions for the laboratory test in Figure 11. The other differences between the two conditions are the water vapor content (10% in the laboratory test is nominally twice that expected in the engine exhaust) and that only one side of the foil is exposed to the exhaust gas in the recuperator. The net is an expected factor of 2 increase in Cr loss in the recuperator compared to the laboratory test. Unfortunately, the depletion from the current specimens are not significant enough to reliably quantify using the current EPMA technique to verify the

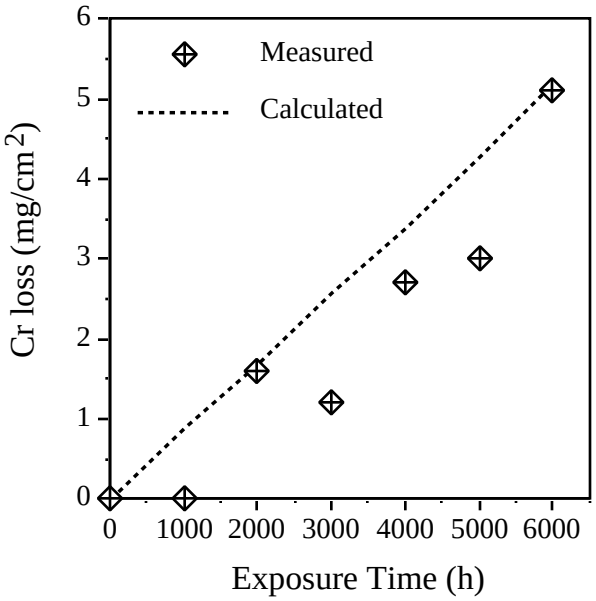


Figure 10. Comparison of the calculated and measured Cr loss from alloy 709 foils exposed to humid air at 800°C.

difference between these conditions.

## DISCUSSION

A correlation between laboratory and engine testing is one of the final unresolved issues remaining in quantifying the degradation of austenitic steels in the recuperator environment. The present mechanistic model suggests that Cr is being lost at a linear rate due to the formation of $CrO_2(OH)_2$. Once the alloy is depleted in Cr, accelerated attack occurs resulting in $FeO_x$ nodule formation and rapid loss of metal which cannot be tolerated in a thin-walled recuperator. The linear kinetics of this mechanism allow the 10,000h laboratory data to be easily extrapolated to a 40,000h or longer exposure. However, the conditions in the recuperator are significantly different than those in the laboratory test and Cr depletion rates are needed as a function of temperature to predict lifetimes in the recuperator application.

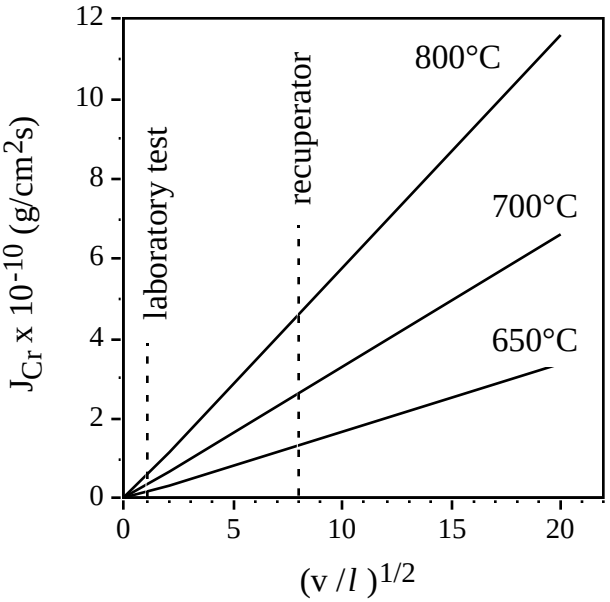


Figure 11. Calculated Cr loss fluxes as a function of $(v/l)^{1/2}$ for air+5%$H_2O$ at 650°-800°C. Dashed lines mark conditions in the laboratory test compared to the approximate conditions in a recuperator.

Because of the much higher gas velocity in the recuperator, it is anticipated that Cr evaporation will be faster in that environment. Due to the difference in v/*l*, the calculation predicted a factor of 8 higher.[21] However, the 10% water vapor in the laboratory test was approximately twice that in exhaust gas. Based on Equation 1, with a constant oxygen partial pressure, the partial pressure of $CrO_2(OH)_2$ should be proportional to the $H_2O$ pressure and thus be reduced by a factor of 2. Also, the laboratory test exposed both sides of the specimen to humid air while only one side is exposed in the recuperator. Thus, a net factor of 2 higher rate in the recuperator was predicted.[21] Comparing the depletion profiles in Figure 7 for the recuperator at 720°C to those in Figure 6b for the 700°C laboratory test qualitatively confirms that the depletion in exhaust gas was faster than in the laboratory test. The loss in the recuperator at 720°C, was similar to the laboratory test at 800°C, Figure 9. However, the standard deviations were very different. Additional profiles need to be measured for the former specimen to obtain a more reliable Cr depletion. However, longer exposures in the microturbine with higher Cr depletion levels will make it much easier to measure the depletion and provide the needed effect of temperature on the rate.

The effect of temperature does not appear as straightforward in the laboratory test as in the microturbine results. In the laboratory tests, the oxide scale and Cr depletion were noticeably higher at 650°C compared to 700°C. This difference may be due to the formation of a higher Cr content oxide at the higher temperature. In general, it would be expected that better selective oxidation of Cr would occur at higher temperature (due to faster Cr diffusion in the alloy), possibly changing the scale from a faster-growing Fe-Cr spinel to a slower-growing chromia. Characterization of the scale on long-term exposures of a FeCr alloy showed this change with temperature,[22] as did short term exposures of NiCr alloys.[23] Thus, a slower-growing oxide may have formed at the higher temperature, resulting in a thinner oxide and less alloy depletion.

The effect of temperature on the evaporation rate also may play a role. Due to the combination of scale growth and evaporation, para-linear kinetics have been observed and should result in a steady-state scale thickness.[24] A typical para-linear reaction is:

$$\frac{dX}{dt} = \frac{k_p}{X} - k_{ev} \qquad [2]$$

where X is the scale thickness, t is time, $k_p$ is the parabolic rate constant for diffusion-controlled scale growth and $k_{ev}$ represents the vaporization loss rate. Once the scale reaches this steady-state thickness, $X_{ss}$ when dX/dt = 0, continued exposure should result in temperature-dependent evaporation controlling further Cr depletion:

$$\Delta M_{Cr} = k_{ev} t + X_{ss} N_{Cr} \qquad [3]$$

where $\Delta M_{Cr}$ is the cumulative mass loss of Cr and $N_{Cr}$ is the concentration of Cr in the scale of thickness $X_{ss}$. Thus at long times

(e.g. <2,000h at 650°C), where changes in $\Delta M_{Cr}$ are dominated by $k_{ev}$ and the specimen mass begins to decrease with time (Figure 2), the effect of temperature on the evaporation rate will eventually be clear. Comparing the Cr depletion levels at 650° and 700°C, the measured depletion was initially lower at 700°C, Figure 9. However, after 10,000h, the amount of Cr loss was higher at 700°C than at 650°C indicating an increase in $k_{ev}$ with temperature.

For the exposures in the microturbine, it was not possible to quantify the exact depletion at the lower temperatures. However, the Cr maps in Figure 8 qualitatively indicate more degradation and associated depletion at 720°C than at the lower temperatures where the depth of grain boundary depletion was lower and fewer and smaller oxide penetrations and nodules formed.

The exact mechanism by which water vapor (or perhaps $H_2$) increases the scale growth rate (e.g. Figure 4) or causes nodule formation on the Cr-depleted substrate has not been determined. However, these mechanisms do not appear to be critical to quantifying the degradation rate. Comparing Figures 3d and 4a, the Cr-rich oxide scale does not appear to increase in thickness much between 5,000 and 10,000h at 700°C in the laboratory test. Thus, most of the Cr being lost from the foil substrate in this time period is likely due to the evaporation mechanism.

The specimens in the exhaust gas exposure also were subject to a hoop stress of ~50MPa. The effect of stress on degradation in this environment has not been well studied. The penetrations observed for these samples in Figure 5 may lead to the assumption that this resulted from the applied stress. However, the same penetrations were observed in the unstressed laboratory specimens, Figure 4. Another assumption is that the applied stress will have a negative effect on performance. In the literature, applied stress has been observed to both increase and decrease the oxidation rate of chromia-forming alloys.[25,26] Where stress resulted in a thinner, more Cr-rich oxidation product, the result was attributed to increased Cr diffusion in the alloy. Enhanced diffusion could be critical in this application where the relatively slow diffusion of Cr in the alloy at 650°C results in the high Cr depletion rates at the foil surface. Thus, this issue needs to be carefully examined to determine the role of stress in this system.

There also is a possibility that other reaction products in the gas stream or impurities affect the rate of corrosion in the microturbine. Species such as CO or $CO_2$ have been shown to internally carburize austenitic steels at these temperatures.[27] Longer term exposures may provide more insight into a potential carburization mechanism. However, higher Cr contents tended to reduce the extent of internal carburization.[27] Regarding fuel impurities or ingested dust, there was no evidence in the current specimens of any surface deposits that may have accelerated the corrosion rate.

If the present model were correct and the Cr depletion rate is twice that of the laboratory test., then the depletions in Table II extrapolate to very high Cr depletions after 40,000h. These results suggest that alloy 120 would lose 50% of its Cr content at 650°C after 40,000h. However, the deviations on these measured values are quite large resulting in an unreliable prediction.

Another factor that needs to be further considered is the eventual formation of a thick Fe-rich oxide layer on almost any austenitic alloy in this application. Based on the nodule formation observed in both experiments, a layer will likely form at some point in service. It is not certain if a continuous Fe-rich oxide layer on the surface could reduce the Cr depletion rate by inhibiting the evaporation of the oxy-hydroxide. However, this layer needs to be considered in modeling recuperator performance in terms of heat transfer, a thick surface oxide may significantly reduce the effectiveness of the recuperator during long-term service.

## SUMMARY

Initial results were presented comparing specimens of commercial 80µm alloy 120 foil exposed in humid air in a low velocity laboratory test to specimens exposed in a the exhaust gas of a 60kW microturbine. After 1,000h in the microturbine exhaust, Cr depletion is clearly evident at the highest exposure temperature. However, the quantification error is sufficiently large that it is difficult to extrapolate the data to longer times or compare it to results for the laboratory test. The same material has been exposed for 5,000h in laboratory testing. Qualitatively, the Cr depletion was higher in the microturbine exposures. However, longer term exposures will make it easier to quantify this difference and provide more information on the effect of temperature on the depletion rate.

## ACKNOWLEDGMENTS

The author would like to thank J. L. Moser, G. W. Garner, H. Longmire and L. R. Walker at ORNL for assistance with the experimental work, D. J. Young, Univ. New South Wales, for developing the model as a visiting scientist at ORNL and D. J. Young, P. J. Maziasz, S. Dryepondt and P. F. Tortorelli for comments on the manuscript. This research was sponsored by the U.S. Department of Energy, Distributed Energy and Electrical Reliability Program under contract DE-AC05-00OR22725 with UT-Battelle, LLC.

## REFERENCES

1. Watts, J. H., 1999, “Microturbines: A New Class of Gas Turbine Engine,” Global Gas Turbine News, **39**(1), pp.4-8.
2. Hamilton, S. L., 2003, The Handbook of Microturbine Generators, PennWell Corp., Tulsa, OK.
3. Maidment, G. G. and Tozer, R. M., 2002 “Combined Cooling Heat and Power in Supermarkets,” Applied Thermal Engineering, **22**, pp.653-65.
4. Pilavachi, P. A., 2002, “Mini- and Micro-Gas Turbines for Combined Heat and Power,” Applied Thermal Engineering, **22**, pp.2003-14.
5. McDonald, C. F., 2003, “Recuperator Considerations for Future Higher Efficiency Microturbines,” Applied Thermal Engineering, **23**, pp.1463-87.
6. Omatete, O., Maziasz, P. J., Pint, B. A. and Stinton, D. P., 2000, “Recuperators for Advanced Microturbines,” Report No.ORNL/TM-2000/304, Oak Ridge National Laboratory, Oak Ridge, TN.
7. Kesseli, J., Wolf, T., Nash, J. and Freedman, S., 2003, “Micro, Industrial, and Advanced Gas Turbines Employing Recuperators,” ASME Paper #GT2003-38938, presented at the International Gas Turbine & Aeroengine Congress & Exhibition, Atlanta, GA, June 2-5, 2003.
8. Pint, B. A. and Rakowski, J. M., 2000, “Effect of Water Vapor on the Oxidation Resistance of Stainless Steels,” NACE Paper 00-259, Houston, TX, presented at NACE Corrosion 2000, Orlando, FL, March 2000.

9. Rakowski, J. M., 2001, “The Oxidation of Austenitic Stainless Steel Foils in Humidified Air,” ASME Paper 2001-GT-360, presented at the International Gas Turbine & Aeroengine Congress & Exhibition, Amsterdam, Netherlands, June 3-6, 2002.
10. Pint, B. A. and More, K. L., 2004, "Stainless Steels with Improved Oxidation Resistance for Recuperators," ASME Paper #GT2004-53627, presented at the International Gas Turbine & Aeroengine Congress & Exhibition, Vienna, Austria, June 14-17, 2004.
11. Asteman, H., Svensson, J.-E., Norell, M. and Johansson, L.-G., 2000, “Influence of Water Vapor and Flow Rate on the High-Temperature Oxidation of 304L; Effect of Chromium Oxide Hydroxide Evaporation,” Oxidation of Metals, **54**, pp.11-26.5.
12. Opila, E. J., 2004, “Volatility of Common Protective Oxides in High-Temperature Water Vapor: Current Understanding and Unanswered Questions,” Materials Science Forum, **461-464**, pp.765-74.
13. Stambler, I., 2004, “Mercury 50 rated at 4600kW and 38.5% efficiency with 5ppm $NO_x$,” Gas Turbine World, Feb-Mar 2004, pp.12-16.
14. Matthews, W. J., Bartel, T., Klarstrom, D. L. and Walker, L. R., 2005 “Engine Testing of an Advanced Alloy for Microturbine Primary Surface Recuperators,” ASME Paper #GT2005-68781, presented at the International Gas Turbine & Aeroengine Congress & Exhibition, Reno-Tahoe, NV, June 6-9, 2005.
15. Kikuchi, M., Sakakibara, M., Otoguro, Y., Mimura, H., Araki, S. and Fujita, T., 1985, “An Austenitic Heat Resisting Steel Tube Developed for Advanced Fossil-Fired Steam Plants,” in High Temperature Alloys, Their Exploitable Potential, J. B. Marriott, M. Merz, J. Nihoul and J. Ward Eds., Elsevier, London, pp.267-76.
16. Rakowski, J. M., Stinner, C. P., Lipschutz, M. and Montague, J. P., 2004, “The Use and Performance of Oxidation and Creep-Resistant Stainless Steels in an Exhaust Gas Primary Surface Recuperator Application,” ASME Paper #GT2004-53917, presented at the International Gas Turbine & Aeroengine Congress & Exhibition, Vienna, Austria, June 14-17, 2004.
17. Pint, B. A.,2005, “The Effect of Water Vapor on Cr Depletion in Advanced Recuperator Alloys,” ASME Paper #GT2005-68495, presented at the International Gas Turbine & Aeroengine Congress & Exhibition, Reno-Tahoe, NV, June 6-9, 2005.
18. Lara-Curzio, E., Maziasz, P. J., Pint, B. A., Stewart, M., Hamrin D., Lipovich, N. and DeMore, D., 2002, “Test Facility for Screening and Evaluating Candidate Materials for Advanced Microturbine Recuperators,” ASME Paper #2002-GT-30581, presented at the International Gas Turbine & Aeroengine Congress & Exhibition, Amsterdam, Netherlands, June 3-6, 2002.
19. Lara-Curzio, E., Trejo, R., More, K. L., Maziasz, P. J. and Pint, B. A., 2005, “Evaluation and Characterization of Iron- and Nickel-Based Alloys for Microturbine Recuperators,” ASME Paper #GT2005-68630, presented at the International Gas Turbine & Aeroengine Congress & Exhibition, Reno-Tahoe, NV, June 6-9, 2005.
20. Maziasz, P. J., Swindeman, R. W., Shingledecker, J. P., More, K. L., Pint, B. A., Lara-Curzio, E. and Evans, N. D., 2003, "Improving High-Temperature Performance of Austenitic Stainless Steels for Advanced Microturbine Recuperators," in Parsons 2003, Engineering Issues in Turbine Machinery, Power Plant and Renewables, Maney, London, pp.1057-73.
21. Young, D. J. and Pint, B. A., 2006, “Chromium Volatilization Rates from $Cr_2O_3$ Scales Into Flowing Gases Containing Water Vapor,” Oxidation of Metals, in press.
22. Hoelzer, D. T., Pint, B. A., Wright, I. G., 2000, "AMicrostructural Study of the Oxide Scale Formation on an ODS Fe-13Cr Alloy," Journal of Nuclear Materials, **283-287**, pp.1306-10.
23. Kumar, L., Venkataramani, R., Sundararaman, M., Mukhopadhyay, P. and Garg, S. P., 1996, “Studies on the Oxidation Behavior of Inconel 625 Between 873 and 1523K,” Oxidation of Metals, **45**, pp.221-44.
24. C. S. Tedmon, 1966, “The Effect of Oxide Volatilization on the Oxidation Kinetics of Cr and Fe-Cr Alloys,” Journal of the Electrochemical Society, **113**, pp.766-8.
25. Calvarin-Amiri, G., Molins, R. and Huntz, A. M., 2001, “Coupling Between Oxidation and Mechanical Stresses. Application to the Oxidation of Ni-20Cr Foils,” Materials Science Forum, **369-372**, pp.467-74.
26. Schmitt, J. F., Pacia, N., Pigeat, P. and Weber, B., 1995, “Study of the Initial Oxidation of a Ni-20Cr Alloy in the Temperature-Range 550-830°C – Influence of Mechanical Deformation,”Oxidation of Metals, **44**, pp.429-52.
27. McCoy, H. E., 1965, “Type 304 Stainless Steel vs. Flowing $CO_2$ at Atmospheric Pressure and 1100-1800°F,” Corrosion, **21**, pp.84-94.